JOURNAL OF GUIDANCE, CONTROL, AND DYNAMICS
Vol. 23, No. 5, September–October 2000

Computational Test Cases for the Benchmark Active Controls Model

Robert M. Bennett,* Robert C. Scott,† and Carol D. Wieseman‡
NASA Langley Research Center, Hampton, Virginia 23681-2199

Unsteady aerodynamic and aeroelastic computational test cases have been selected from the data set for the Benchmark Active Controls Technology model. Data sets for trailing-edge control surface oscillations and upper-surface spoiler oscillations for a range of Mach numbers, angle of attack, and static control deflections are included. Cases also include static angles of attack, static trailing-edge control, and static upper-surface spoiler deflections for a range of conditions near those for the oscillation cases. The aeroelastic test cases include three types of flutter instability and dynamic response measurements for oscillations of the controls on the flexible mount.

Nomenclature

C_p = pressure coefficient, $(p - p_\infty)/q_\infty$
c = wing chord, ft (m)
f = frequency, Hz
k = reduced frequency, $\omega c/(2V_\infty)$
M = Mach number
p = pressure, psf (kPa)
p_∞ = freestream static pressure, psf (kPa)
q = dynamic pressure, psf (kPa)
V_∞ = freestream velocity, ft/s (m/s)
x/c = streamwise fraction of local chord
y = spanwise coordinate normal to freestream
z = vertical coordinate normal to freestream
α_0 = mean angle of attack, deg
γ = ratio of specific heats for test gas
Δ = difference, lower-upper
δ_{ls} = lower spoiler deflection, deg
δ_{te} = trailing-edge control surface deflection, deg
δ_{us} = upper spoiler deflection, deg
η = fraction of span, y/s
θ = pitch angle
ω = frequency, rad/s

Subscripts

mean = mean value
z = plunge mode
θ = pitch mode
0 = steady value
∞ = freestream value

Introduction

As a portion of the Benchmark Models Program[1,2] at NASA Langley Research Center, a simple generic model was developed for active controls research, called the Benchmark Active Controls Technology (BACT) model. This model was based on the previously tested benchmark models rectangular wing with the NACA 0012 airfoil section that was mounted on the pitch and plunge apparatus (PAPA) for flutter testing.[1,3–5] The BACT model had an upper surface spoiler, a lower surface spoiler, and a trailing-edge control surface for use in flutter suppression and dynamic response excitation. Previous experience with flutter suppression[6,7] indicated a need for measured control surface aerodynamics to design control laws accurately. Three different types of flutter instability boundaries had also been determined for the NACA 0012/PAPA model,[1,3–5] a classical flutter boundary, a transonic stall flutter boundary at angle of attack, and a plunge instability near $M = 0.9$. Therefore, an extensive set of steady and control surface oscillation data was generated spanning the range of the three types of instabilities.[8] This information was subsequently used to design control laws to suppress flutter.

There have been three tests of the BACT model in the NASA Langley Research Center Transonic Dynamics Tunnel (TDT). The objectives of the first test, TDT test 485, were to generate a data set of steady and unsteady control surface effectiveness data, to determine the flutter boundaries on the PAPA mount, and to determine the open-loop dynamic characteristics of the control systems including the actuators. Unsteady pressures, loads, and transfer functions were measured using a rigid mount system with a balance for aerodynamic loads, whereas the flutter tests were conducted on the flexible PAPA mount system. The other two tests, TDT test 502 and TDT test 518, were performed on PAPA only and were primarily oriented toward active controls research with some flutter data obtained to supplement the data from test 485. During these tests of BACT, a rather unique and extensive database of over 3000 data sets was acquired involving a wide variety of types of data.

Efforts have been made in the past to provide experimental unsteady aerodynamic test cases for use in comparisons with the results of computational methods. A notable example[9,10] included a number of configurations. Many of the configurations[9] were simple two-dimensional airfoils, but the data have been very useful in development of computer programs for computational aeroelasticity. To update and extend the range of available data sets, there have been recent efforts to provide a compendium of additional data for a broader range of conditions including flutter, dynamic stall, and other unsteady aerodynamic phenomena.[11] This volume was compiled by the Applied Vehicle Technology Working Group 003 under the NATO Research and Technology Organization. Several types of data from the BACT model were included in this effort. An overview of the test cases from BACT that have been selected[11] to illustrate critical trends is given here to assist aerodynamic and aeroelastic computational comparisons. The test cases are numbered using a system that should facilitate reference to the individual cases for comparison by computational investigators.

In this effort several test cases are selected to illustrate trends for a variety of different conditions with emphasis on transonic flow effects. Cases for static angles of attack, static trailing-edge control, and upper-surface spoiler deflections are included for a range of conditions near those for the oscillation cases. Cases for oscillations of the trailing-edge control and upper-surface spoiler

Received 5 August 1999; revision received 11 January 2000; accepted for publication 3 March 2000.

*Senior Aerospace Engineer, Aeroelasticity Branch, Mail Stop 340. Associate Fellow AIAA.
†Aerospace Engineer, Aeroelasticity Branch, Mail Stop 340. Senior Member AIAA.
‡Aerospace Engineer, Aeroelasticity Branch, Mail Stop 340. Associate Fellow AIAA.

for a range of oscillation frequency, Mach number, angle of attack, and static control deflection are included. Cases for all three types of flutter instability are selected. In addition, some aeroelastic test cases are included for dynamic response measurements during forced oscillations of the controls on the flexible mount. Only a brief overview of the model and tests that may be pertinent to computational efforts is given because they have been more fully described in the accompanying paper of this issue.[8] Included are the model dimensions, description of the mounting systems, and photograph of the wind-tunnel installation, which are not repeated here.

Some aerodynamic comparisons with the BACT data have been made using linear theory and computational fluid dynamics codes at the Navier–Stokes level.[12–15] Some mechanical and active control studies also have been presented.[16–21]

Only the static pressures and the first harmonic real and imaginary parts of the pressures are included in the data for the test cases, but digitized time histories have been archived. The data for the test cases are also available as separate electronic files. The reference document[11] also includes a formulary or table that elaborates on some of the test and model details.

Model and Tests

The BACT model was tested in the NASA Langley Research Center TDT. The tunnel has a slotted test section 16 ft (4.064 m) square with cropped corners. At the time of these tests, it could be operated with air or a heavy gas, R-12, as a test medium at pressures from very low to near atmospheric values. Currently, the TDT can be operated with air or R-134a as a test medium. An early description of this facility[22] is available, and more recent descriptions of the facility have been presented.[23,24] The description of an early data system[25] and the recent data system[26,27] are published, but the data acquisition system used in the BACT tests was a version between these systems. Based on the results of measurements of transition on a cone,[28,29] the turbulence level for this tunnel is in the average large transonic tunnel category. Some low-speed turbulence measurements in air have also been made.[30]

The BACT model[8,11] is a rectangular planform wing with a span of 32 in. (813 mm) plus a tip of revolution and a chord of 16 in. (406 mm). It has a trailing-edge control surface of 25% chord, hinged at 75% chord, extending between 45 and 75% span. Upper and lower surface spoilers of 15% chord length were located directly ahead of the trailing-edge control surface, were of the same span, and were hinged at 60% chord. The outward surface of the spoilers was flat, and a relatively thin trailing edge extended to near the round leading-edge radius of the trailing-edge control surface. When both spoilers were deployed, the cavity underneath was open, permitting flow between upper and lower surfaces. The cavity contained plumbing for the actuators and wiring, and the shape is undocumented. The wing was machined from aluminum and was very smooth and was tested with a transition strip at 5% chord. The control surfaces were of composite construction and were driven with miniature hydraulic actuators located within the wing.

The BACT model was mounted on a large splitter plate set out approximately 40 in. (1.02 m) from tunnel sidewall.[8] The model had an end plate fixed to its root that moved with the model within a recessed or undercut section of the splitter plate. A large fairing behind the splitter plate isolated the equipment between the splitter plate and the tunnel sidewall from the airstream. Some recent tests[31] of the splitter plate arrangement without a wing have shown some nonuniformity of the flow resulting from the flow around the splitter plate leading edge for Mach numbers above $M = 0.80$, and the data may be somewhat affected.

The BACT model was tested with two different mounting systems. For the first test, TDT test 485, a circular strut extended from the turntable to the balance that was attached to the wing for force measurements. The model could be pitched statically with the turntable, and the controls were powered for static and dynamic measurements. The test cases for control surface static deflection and oscillation were determined from this setup.

The model was also tested using PAPA.[32,33] The PAPA system permits rigid-body pitch and plunge motion of the wing and flutter of the system by the use of four circular rods for flexibility. This system has sufficient strength to permit flutter testing at moderate angles of attack including some stall flutter cases. The rods are arranged such that the elastic axis is at the midchord and the model is balanced to place the center of gravity on the midchord. The system thus gives primarily pitch and plunge uncoupled modes about the midchord of the model. The summary of the modal parameters is given in Table 1. The generalized masses given here are the effective mass and pitch inertia calculated from the frequency and stiffness values. Higher modes of this system have been explored and presented[34] with a different model. Some amplitude effects on frequency and damping were presented,[34] but may not apply to BACT as a result of the addition of hydraulic lines spanning the PAPA system. Detailed windoff free decay records have been archived. A remotely operable restraining or snubber system was installed and was used to suppress flutter when it grew near the amplitude limits, and many flutter points were obtained. Some additional mass parameters relating to the control surfaces are available.[16–18]

Both the model and the plate that constrains the model end of the PAPA system are large in mass. The resulting mass ratio at flutter is, thus, very large, and consequently the reduced frequency at flutter is very low. The flutter crossings are relatively mild and unpublished calculations have indicated some sensitivity to torsional aerodynamic damping.

The model was instrumented for unsteady pressures at two chords and for dynamic motions. The list of transducers is given in Table 2. There were 58 unsteady pressure transducers located along the chord at 60% span that is at the midspan of the control surfaces. There were five transducers on each spoiler and seven on each of the upper and lower surfaces of the trailing-edge control surface. This relatively dense spacing of the transducers was selected to define the pressures near the control surface hinge lines. In addition there were 17 unsteady pressure transducers located at 40% span over the aft portion of the chord that were placed to examine the carryover loading near the side edge of the control surfaces. Space limitations prevented further pressure instrumentation at other chords. Note that some flow visualization work on these low-aspect-ratio planforms indicated that wing surface separation tended to occur in a cellular fashion on the aft inboard portion of the wing. The row of pressure transducers at 60% chord was near the outer portion of this separated flow cell for some of the separated flow cases.

Dynamic data from all channels were acquired simultaneously at a rate of 500 samples/s and stored in digital form on disk. For

Table 1 Measured nominal structural dynamic parameters

Parameter	Plunge mode	Pitch mode
Frequency	3.34 Hz	5.21 Hz
Stiffness	2,686 lb/ft	3,000 ft-lb/rad
Damping ratio ς	0.0014	0.0010
Effective mass or inertia	6.08 slug	2.80 slug-ft^2

Table 2 Instrumentation

Instrument	Quantity
Model pressure transducers	75
Splitter plate pressure transducers (test 485 only)	20
Boundary-layer rake pressure transducers (test 485 only)	10
Model accelerometers	4
Control surface accelerometers	6
Control surface potentiometers	3
Control surface command signals	3
Hydraulic pressure transducers	6
Balance components (rigid support only)	5
PAPA strain gauge bridges (flexible support only)	2
PAPA accelerometers (flexible support only)	2
Turntable angle-of-attack accelerometer	1
Model angle-of-attack accelerometer	1

the static data, at least 10 s of data were acquired for averaging, and, for the oscillating control cases, 8–10 s of data were acquired and analyzed. For the flutter cases, data were selected for nearly constant amplitude and ran from 3 to 30 s. Each recorded data set was assigned an index called a point number, which is given in the Tables 3–10. Although it was intended to use 200-Hz low-pass filters in the data stream prior to digitizing the data to avoid aliasing, the filters were later thought to be set at 1000 Hz as a result of a data system problem. The data are, thus, considered aliased with a foldover frequency of 250 Hz. For the flutter data, which were in the 4–10 Hz range, for the first harmonic to be contaminated, there would have to be significant signals at 990–996 or at 490–496 Hz. It is not considered likely that there are significant disturbances in these frequency ranges.

Detailed geometry measurements were performed for this wing along several sections. The measured ordinates are not included herein, but are available as an electronic file.

Test Cases

An extensive set of test cases is selected with emphasis on transonic flow effects. The test cases are numbered by a four or five character identifier. The scheme is indicated by the following diagram.

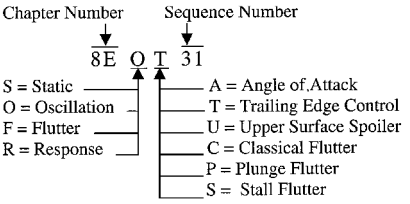

Table 3 Static test cases for angle of attack

Test case no.	Test	Run	Point no.	M	q, psf	α, deg	δ_{te_0}, deg	δ_{us_0}, deg	δ_{ls_0}, deg
8ESA1	485	27	1911	0.650	145.0	−0.03	0.3	0.2	0.2
8ESA2	485	27	1912	0.648	144.2	0.51	0.3	0.2	0.2
8ESA3	485	27	1913	0.650	144.8	1.01	0.3	0.2	0.2
8ESA4	485	27	1914	0.650	145.1	2.05	0.3	0.2	0.2
8ESA5	485	27	1915	0.649	144.6	3.99	0.3	0.2	0.2
8ESA6	485	27	1916	0.651	145.3	6.01	0.3	0.2	0.2
8ESA7	485	27	1917	0.650	145.1	−2.01	0.3	0.2	0.2
8ESA8	485	27	1918	0.649	144.8	−4.01	0.3	0.2	0.2
8ESA9	485	5	136	0.768	140.4	−0.01	0.0	0.2	0.0
8ESA10	485	5	137	0.771	141.6	0.51	0.0	0.2	0.0
8ESA11	485	5	138	0.772	142.1	1.01	0.0	0.2	0.0
8ESA12	485	5	139	0.769	141.6	2.00	0.0	0.2	0.0
8ESA13	485	5	140	0.769	141.7	3.01	0.0	0.2	0.0
8ESA14	485	5	141	0.768	141.5	3.99	0.0	0.2	0.0
8ESA15	485	5	142	0.769	141.7	5.00	0.0	0.2	0.0
8ESA16	485	5	143	0.770	142.3	6.01	0.0	0.2	0.0
8ESA17	485	5	144	0.768	141.7	7.02	0.0	0.2	0.0
8ESA18	485	5	145	0.769	142.2	8.02	0.0	0.2	0.0
8ESA19	485	5	146	0.769	142.2	9.00	0.0	0.1	0.0
8ESA20	485	5	147	0.770	142.6	6.02	0.0	0.2	0.0
8ESA21	485	5	148	0.769	142.6	4.02	0.0	0.2	0.0
8ESA22	485	5	150	0.769	142.8	−0.03	0.0	0.1	0.0
8ESA23	485	5	151	0.769	142.8	−2.02	0.0	0.1	0.0
8ESA24	485	5	152	0.769	142.9	−4.02	0.0	0.1	0.0
8ESA25	485	21	1405	0.821	169.2	−0.01	0.3	0.2	0.2
8ESA26	485	21	1406	0.817	168.5	0.50	0.3	0.2	0.2
8ESA27	485	21	1407	0.817	168.5	1.03	0.3	0.2	0.2
8ESA28	485	21	1408	0.819	169.0	2.05	0.3	0.2	0.2
8ESA29	485	21	1409	0.819	169.1	3.12	0.3	0.2	0.2
8ESA30	485	21	1410	0.821	169.9	3.99	0.3	0.2	0.2
8ESA31	485	21	1411	0.819	169.5	5.01	0.3	0.2	0.2
8ESA32	485	21	1412	0.819	169.4	6.00	0.3	0.2	0.2
8ESA33	485	21	1413	0.819	169.4	7.04	0.3	0.2	0.2
8ESA34	485	21	1414	0.820	169.7	8.04	0.3	0.1	0.2
8ESA35	485	21	1415	0.819	169.6	9.04	0.3	0.1	0.2
8ESA36	485	21	1416	0.819	169.8	10.04	0.3	0.1	0.2
8ESA37	485	21	1418	0.816	169.2	6.01	0.3	0.2	0.2
8ESA38	485	21	1420	0.818	169.7	1.99	0.3	0.2	0.2
8ESA39	485	21	1421	0.818	169.8	−0.06	0.3	0.2	0.2
8ESA40	485	21	1423	0.818	169.8	−4.01	0.3	0.2	0.2
8ESA41	485	25	1715	0.902	134.5	0.00	0.2	0.3	0.1
8ESA42	485	25	1716	0.903	134.7	0.26	0.2	0.4	0.1
8ESA43	485	25	1717	0.899	134.0	0.50	0.2	0.4	0.2
8ESA44	485	25	1718	0.900	134.2	0.75	0.2	0.3	0.4
8ESA45	485	25	1719	0.902	134.7	1.02	0.2	0.3	0.4
8ESA46	485	25	1720	0.897	133.9	1.52	0.2	0.4	0.5
8ESA47	485	25	1721	0.899	134.4	2.00	0.2	0.3	0.4
8ESA48	485	25	1722	0.896	133.9	3.01	0.2	0.3	0.4

Table 4 Static test cases for trailing-edge control surface deflection

Test case no.	Test	Run	Point no.	M	q, psf	α, deg	δ_{te_0}, deg	δ_{us_0}, deg	δ_{ls_0}, deg
8EST1	485	27	1929	0.649	145.0	0.01	−9.7	0.2	0.2
8EST2	485	27	1930	0.648	144.8	0.01	−4.8	0.2	0.4
8EST3	485	27	1931	0.648	144.7	0.01	−1.7	0.2	0.2
8EST4	485	27	1932	0.648	144.7	0.01	0.3	0.2	0.3
8EST5	485	27	1933	0.650	145.4	0.01	2.3	0.2	0.3
8EST6	485	27	1934	0.650	145.2	0.01	5.3	0.2	0.2
8EST7	485	27	1935	0.651	145.6	0.01	10.3	0.2	0.2
8EST8	485	27	1937	0.649	145.1	1.99	−9.8	0.2	0.1
8EST9	485	27	1938	0.650	145.4	1.99	−4.8	0.2	0.2
8EST10	485	27	1939	0.650	145.3	1.99	−1.7	0.2	0.1
8EST11	485	27	1940	0.650	145.4	1.99	0.3	0.2	0.1
8EST12	485	27	1941	0.650	145.6	1.99	2.3	0.2	0.2
8EST13	485	27	1942	0.649	145.3	1.99	5.3	0.2	0.2
8EST14	485	27	1943	0.649	145.3	1.99	10.3	0.2	0.2
8EST15	485	5	156	0.767	142.9	0.03	−10.0	0.1	−0.1
8EST16	485	5	157	0.768	143.1	0.03	−5.0	0.1	−0.1
8EST17	485	5	158	0.771	143.9	0.03	−2.0	0.1	−0.1
8EST18	485	5	159	0.768	143.1	0.03	0.0	0.1	−0.1
8EST19	485	5	160	0.772	144.4	0.03	0.5	0.1	−0.1
8EST20	485	5	161	0.769	143.5	0.03	1.0	0.1	−0.1
8EST21	485	5	162	0.768	143.4	0.03	2.0	0.1	−0.1
8EST22	485	5	163	0.770	143.9	0.03	3.0	0.1	0.0
8EST23	485	5	164	0.769	143.7	0.03	5.0	0.1	0.0
8EST24	485	5	165	0.770	144.1	0.03	10.0	0.1	−0.1
8EST25	485	5	166	0.770	144.1	0.03	12.0	0.1	−0.1
8EST26	485	5	193	0.770	145.2	3.99	−9.9	0.1	−0.1
8EST27	485	5	195	0.769	145.1	3.99	−5.0	0.1	−0.1
8EST28	485	5	196	0.770	145.5	3.99	−1.9	0.1	−0.1
8EST29	485	5	197	0.769	145.3	3.99	0.0	0.1	−0.1
8EST30	485	5	200	0.768	145.1	3.99	1.0	0.1	−0.1
8EST31	485	5	201	0.769	145.3	3.99	2.0	0.1	−0.1
8EST32	485	5	202	0.770	145.6	3.99	3.0	0.1	−0.1
8EST33	485	5	203	0.769	145.4	3.99	5.0	0.1	−0.1
8EST34	485	5	204	0.769	145.4	3.99	10.0	0.1	−0.1
8EST35	485	5	205	0.770	145.6	3.99	12.0	0.1	−0.1
8EST36	485	21	1425	0.818	170.0	0.03	−9.7	−0.2	0.2
8EST37	485	21	1426	0.820	170.6	0.03	−4.7	−0.1	0.2
8EST38	485	21	1427	0.818	170.0	0.03	−1.7	−0.1	0.2
8EST39	485	21	1428	0.817	170.0	0.03	0.3	−0.1	0.2
8EST40	485	21	1429	0.820	170.7	0.03	1.3	−0.1	0.2
8EST41	485	21	1430	0.819	170.5	0.03	2.3	−0.1	0.2
8EST42	485	21	1431	0.818	170.3	0.03	3.3	−0.1	0.2
8EST43	485	21	1432	0.817	170.0	0.03	5.3	−0.1	0.2
8EST44	485	21	1433	0.818	170.3	0.03	10.3	−0.1	0.2
8EST45	485	21	1434	0.821	171.1	0.03	12.3	−0.1	0.2
8EST46	485	21	1447	0.817	170.3	4.01	−9.7	−0.1	0.2
8EST47	485	21	1448	0.819	170.9	4.01	−4.7	−0.1	0.2
8EST48	485	21	1449	0.818	170.8	4.01	−1.7	−0.1	0.2
8EST49	485	21	1450	0.817	170.5	4.01	0.3	−0.1	0.2
8EST50	485	21	1451	0.817	170.7	4.01	1.3	−0.1	0.2
8EST51	485	21	1452	0.818	170.9	4.01	2.3	−0.1	0.2
8EST52	485	21	1453	0.818	170.9	4.01	3.4	−0.1	0.2
8EST53	485	21	1454	0.817	170.5	4.01	5.4	−0.1	0.2
8EST54	485	21	1455	0.816	170.3	4.01	10.3	−0.1	0.2
8EST55	485	21	1456	0.818	170.8	4.00	12.3	−0.1	0.2
8EST56	485	25	1735	0.896	134.9	−0.05	−4.8	0.3	0.3
8EST57	485	25	1737	0.899	135.6	−0.05	−1.7	0.2	0.3
8EST58	485	25	1738	0.896	135.2	−0.05	−0.7	0.2	0.3
8EST59	485	25	1739	0.896	135.2	−0.05	−0.3	0.2	0.3
8EST60	485	25	1740	0.897	135.3	−0.05	0.3	0.2	0.3
8EST61	485	25	1741	0.897	135.4	−0.05	0.7	0.2	0.3
8EST62	485	25	1742	0.898	135.5	−0.05	1.3	0.2	0.3
8EST63	485	25	1745	0.897	135.7	−0.05	1.8	0.2	0.2
8EST64	485	25	1746	0.899	136.0	−0.05	2.2	0.2	0.1
8EST65	485	25	1747	0.901	136.4	−0.05	5.2	0.3	0.1

Table 5 Static test cases for upper spoiler deflection

Test case no.	Test	Run	Point no.	M	q, psf	α, deg	δ_{te_0}, deg	δ_{us_0}, deg	δ_{ls_0}, deg
8ESU1	485	27	1953	0.648	145.0	0.00	0.2	0.2	0.2
8ESU2	485	27	1954	0.649	145.3	0.00	0.2	−4.8	0.2
8ESU3	485	27	1955	0.649	145.5	0.00	0.2	−9.8	0.2
8ESU4	485	27	1956	0.648	144.9	0.00	0.2	−20.0	0.2
8ESU5	485	27	1957	0.649	145.4	0.00	0.2	−40.1	0.2
8ESU6	485	27	1959	0.649	145.6	3.98	0.2	0.3	0.2
8ESU7	485	27	1960	0.647	145.0	3.98	0.2	−4.8	0.2
8ESU8	485	27	1961	0.649	145.4	3.98	0.2	−9.8	0.2
8ESU9	485	27	1962	0.649	145.6	3.98	0.2	−19.9	0.2
8ESU10	485	27	1963	0.649	145.5	3.98	0.2	−40.2	0.2
8ESU11	485	8	361	0.771	146.4	−0.01	0.0	−0.2	0.0
8ESU12	485	8	362	0.775	146.7	−0.01	0.0	−0.5	0.0
8ESU13	485	8	363	0.772	146.0	−0.01	0.0	−0.5	0.0
8ESU14	485	8	364	0.772	145.9	−0.01	0.1	−1.0	0.0
8ESU15	485	8	365	0.770	145.6	−0.01	0.1	−2.0	0.0
8ESU16	485	8	366	0.770	145.6	−0.01	0.1	−5.0	0.0
8ESU17	485	8	367	0.772	146.3	−0.01	0.0	−9.9	0.0
8ESU18	485	8	368	0.769	145.5	−0.01	0.0	−15.0	0.0
8ESU19	485	8	369	0.770	146.0	−0.01	0.0	−20.0	0.0
8ESU20	485	8	370	0.770	146.0	−0.01	0.0	−25.0	0.0
8ESU21	485	8	371	0.772	146.9	−0.02	0.0	−35.1	0.0
8ESU22	485	21	1458	0.817	171.0	−0.02	0.3	−0.1	0.1
8ESU23	485	21	1459	0.816	170.6	−0.03	0.3	−0.9	0.2
8ESU24	485	21	1460	0.819	171.3	−0.03	0.3	−2.0	0.2
8ESU25	485	21	1461	0.818	171.4	−0.03	0.3	−4.9	0.2
8ESU26	485	21	1462	0.820	171.8	−0.03	0.3	−10.0	0.2
8ESU27	485	21	1463	0.818	171.2	−0.03	0.3	−14.9	0.2
8ESU28	485	21	1464	0.817	171.0	−0.03	0.3	−19.8	0.2
8ESU29	485	25	1775	0.899	137.2	−0.03	0.2	0.3	0.3
8ESU30	485	25	1776	0.897	137.1	−0.03	0.3	−0.9	0.3
8ESU31	485	25	1777	0.895	136.9	−0.03	0.2	−2.0	0.3
8ESU32	485	25	1778	0.897	137.1	−0.03	0.3	−3.0	0.2

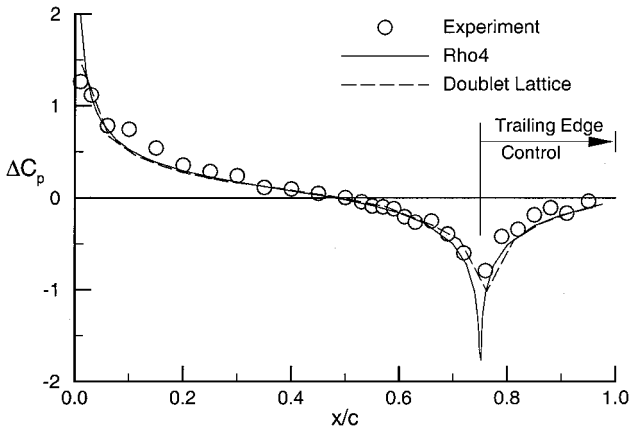

a) M = 0.65, test 485, point 1945

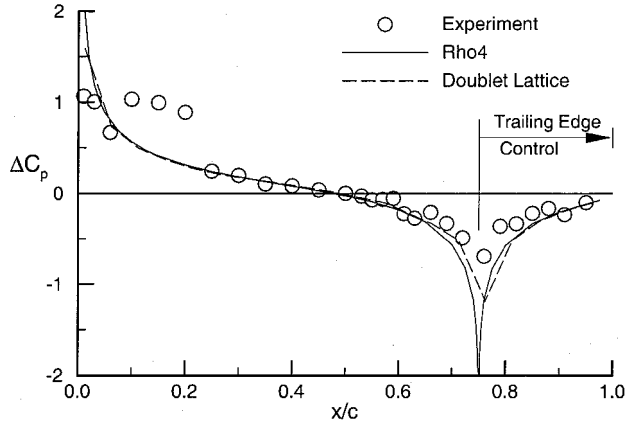

b) M = 0.75, test 485, point 1686

Fig. 1 Comparison of BACT static results with linear aerodynamics, α = 4 deg and $\delta_{te_0} = -10$ deg.

The chapter number is 8E for the chapter identifier of the reference document.[11] The other characters indicate the type or category of the data for the test case and the sequence within the data type. There are several configurations and variables such that a few cases per configuration result in a fairly large number, but one would normally not be concerned with all configurations. The aerodynamic test cases generally include four Mach numbers, $M = 0.65$, which is subsonic at low angles of attack; $M = 0.77$, which is transonic; and near the bottom of the flutter bucket; $M = 0.82$, which is strongly transonic; and $M = 0.90$, which is significantly beyond normal applications for this airfoil. Control surface deflections cases are generally selected

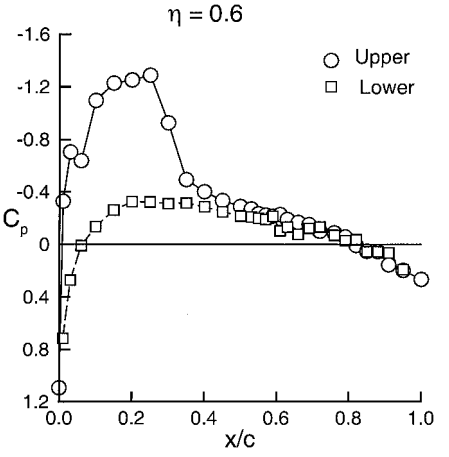

a) Mean pressure coefficient during control surface oscillation

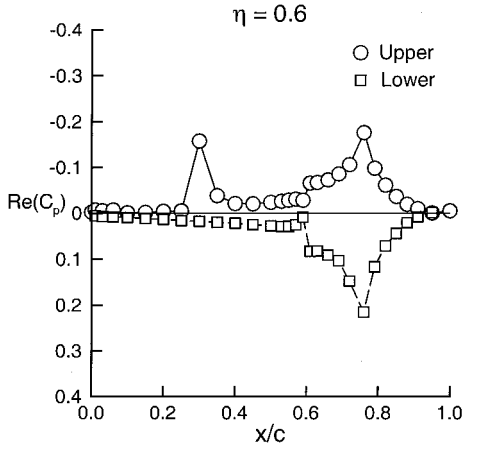

b) Real part of pressure coefficient during control surface oscillation

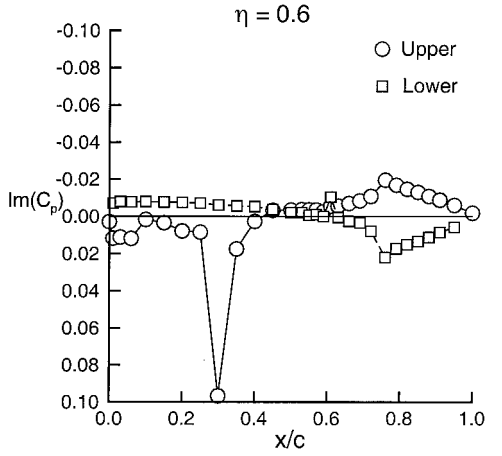

c) Imaginary part of pressure coefficient during control surface oscillation

Fig. 2 Unsteady pressures measured during trailing-edge control oscillations, test case 8EOT31, M = 0.77, α = 4 deg, and f = 10.02 Hz.

Table 6 Test cases for trailing-edge control surface oscillation, $\delta_{us_0} = 0$

Test case no.	Test	Run	Point no.	M	q, psf	α, deg	δ_{te_0}, deg	δ_{te}, deg	k	f, Hz
8EOT1	485	27	1966	0.648	145.3	0.04	0.25	4.05	0.0257	2.00
8EOT2	485	27	1967	0.648	145.2	0.09	0.27	4.04	0.0645	5.01
8EOT3	485	27	1968	0.647	145.1	0.05	0.27	3.83	0.1291	10.02
8EOT4	485	27	1972	0.648	145.5	4.03	0.25	4.05	0.0257	2.00
8EOT5	485	27	1973	0.647	145.1	4.02	0.27	4.04	0.0646	5.01
8EOT6	485	27	1974	0.648	145.5	4.00	0.27	3.83	0.1289	10.02
8EOT7	485	14	901	0.768	151.2	−0.03	0.05	1.07	0.1076	9.93
8EOT8	485	14	904	0.767	151.4	0.04	0.05	2.04	0.0108	1.00
8EOT9	485	14	905	0.768	151.6	−0.06	0.05	2.05	0.0217	2.00
8EOT10	485	14	906	0.769	152.0	0.07	0.05	2.05	0.0325	3.00
8EOT11	485	14	907	0.769	151.9	0.01	0.05	2.06	0.0431	3.99
8EOT12	485	14	908	0.766	151.2	0.04	0.05	2.07	0.0544	5.01
8EOT13	485	14	909	0.768	152.0	−0.06	0.06	2.08	0.0650	6.00
8EOT14	485	14	910	0.769	152.2	0.04	0.08	2.08	0.0868	8.03
8EOT15	485	14	911	0.768	151.8	−0.02	0.08	2.07	0.1076	9.93
8EOT16	485	14	916	0.770	152.6	0.13	0.08	3.00	0.1073	9.93
8EOT17	485	14	919	0.769	152.5	0.07	0.07	4.06	0.0216	2.00
8EOT18	485	14	920	0.769	152.6	0.10	0.08	4.06	0.0542	5.01
8EOT19	485	14	921	0.769	152.6	0.12	0.08	3.89	0.1074	9.93
8EOT20	485	14	933	0.769	153.3	−0.04	5.09	2.03	0.1073	9.93
8EOT21	485	14	936	0.768	153.1	−0.03	5.08	4.05	0.0216	2.00
8EOT22	485	14	937	0.768	153.1	−0.03	5.10	4.03	0.0542	5.01
8EOT23	485	14	938	0.768	153.0	−0.02	5.08	3.84	0.1075	9.93
8EOT24	485	16	1049	0.765	145.0	2.01	0.08	4.05	0.0218	2.00
8EOT25	485	16	1050	0.767	145.4	2.04	0.10	4.05	0.0544	5.01
8EOT26	485	16	1051	0.768	145.8	2.08	0.10	3.88	0.1086	10.02
8EOT27	485	17	1083	0.767	147.4	4.10	0.09	1.07	0.1088	10.02
8EOT28	485	17	1088	0.768	148.0	4.04	0.09	2.05	0.1086	10.02
8EOT29	485	17	1092	0.769	148.3	4.05	0.08	4.04	0.0217	2.00
8EOT30	485	17	1093	0.768	148.3	4.15	0.10	4.04	0.0543	5.01
8EOT31	485	17	1094	0.771	149.0	4.01	0.10	3.87	0.1083	10.02
8EOT32	485	17	1121	0.767	148.7	4.99	0.08	4.04	0.0217	2.00
8EOT33	485	17	1124	0.767	149.1	4.93	0.09	4.04	0.0543	5.01
8EOT34	485	17	1126	0.767	149.2	5.08	0.10	3.87	0.1087	10.02
8EOT35	485	18	1165	0.769	151.8	5.93	0.08	4.04	0.0217	2.00
8EOT36	485	18	1166	0.770	152.2	5.87	0.10	4.04	0.0542	5.01
8EOT37	485	18	1167	0.767	151.4	5.98	0.10	3.87	0.1088	10.02
8EOT38	485	22	1557	0.818	175.2	0.02	0.04	4.04	0.0204	2.00
8EOT39	485	22	1558	0.819	175.2	0.03	0.05	4.04	0.0510	5.01
8EOT40	485	22	1560	0.819	175.4	0.06	0.06	3.88	0.1019	10.02
8EOT41	485	22	1568	0.817	175.2	3.97	0.04	4.04	0.0204	2.00
8EOT42	485	22	1569	0.817	175.1	3.97	0.06	4.04	0.0511	5.01
8EOT43	485	22	1570	0.817	175.1	4.03	0.07	3.86	0.1022	10.02
8EOT44	485	25	1789	0.900	138.5	−0.19	0.25	2.04	0.0186	2.00
8EOT45	485	25	1790	0.899	138.3	−0.23	0.25	2.06	0.0466	5.01
8EOT46	485	25	1791	0.898	138.2	−0.21	0.26	2.06	0.0934	10.02
8EOT47	485	25	1798	0.898	138.4	0.34	0.26	2.05	0.0933	10.02

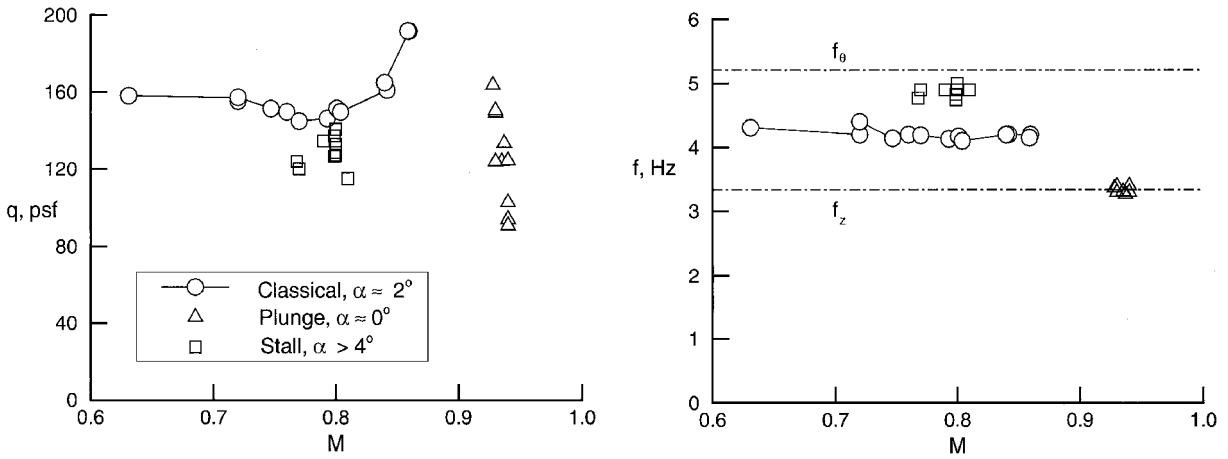

a) Flutter dynamic pressure **b) Flutter frequencies**

Fig. 3 BACT flutter instabilities.

Table 7 Test cases for upper spoiler oscillations, $\delta_{te_0} = 0$

Test case no.	Test	Run	Point no.	M	q, psf	α, deg	δ_{us_0}, deg	δ_{us}, deg	k	f, Hz
8EOU1	485	27	1978	0.648	145.5	−0.02	−9.86	2.12	0.0257	2.00
8EOU2	485	27	1979	0.648	145.4	−0.02	−9.84	2.17	0.0645	5.01
8EOU3	485	27	1980	0.647	145.3	−0.02	−9.82	2.29	0.1291	10.02
8EOU4	485	27	1988	0.648	145.7	3.99	−10.60	2.17	0.0257	2.00
8EOU5	485	27	1989	0.648	145.7	3.99	−10.58	2.21	0.0645	5.01
8EOU6	485	27	1990	0.648	145.9	3.99	−10.54	2.37	0.1289	10.02
8EOU7	485	18	1188	0.769	152.7	−0.01	−5.06	2.36	0.1085	10.02
8EOU8	485	18	1197	0.770	153.1	−0.01	−5.01	4.47	0.1084	10.02
8EOU9	485	18	1201	0.769	153.0	−0.01	−10.06	2.10	0.0216	2.00
8EOU10	485	18	1202	0.769	153.0	−0.01	−10.04	2.16	0.0543	5.01
8EOU11	485	18	1203	0.768	152.6	−0.01	−10.02	2.26	0.1087	10.02
8EOU12	485	18	1207	0.769	153.2	−0.01	−10.09	10.44	0.1085	10.02
8EOU13	485	18	1211	0.768	152.9	−0.01	−20.01	2.09	0.0217	2.00
8EOU14	485	18	1212	0.768	153.0	−0.01	−20.00	2.05	0.0543	5.01
8EOU15	485	18	1213	0.768	152.9	−0.01	−19.97	2.10	0.1086	10.02
8EOU16	485	18	1217	0.769	153.4	−0.01	−19.65	10.18	0.1085	10.02
8EOU17	485	20	1369	0.768	150.7	5.01	−19.52	10.25	0.1086	10.02
8EOU18	485	22	1574	0.818	175.6	0.00	−9.94	2.15	0.0204	2.00
8EOU19	485	22	1575	0.819	176.1	0.00	−9.93	2.18	0.0509	5.01
8EOU20	485	22	1576	0.818	175.8	0.00	−9.90	2.27	0.1020	10.02
8EOU21	485	22	1580	0.819	176.0	0.00	−10.09	10.36	0.1020	10.02
8EOU22	485	22	1584	0.815	174.9	0.00	−19.89	2.11	0.0204	2.00
8EOU23	485	22	1585	0.818	175.8	0.00	−19.89	2.08	0.0510	5.01
8EOU24	485	22	1586	0.819	176.4	0.00	−19.84	2.14	0.1019	10.02
8EOU25	485	22	1590	0.819	176.3	0.00	−19.43	10.15	0.1020	10.02
8EOU26	485	23	1618	0.819	177.4	4.01	−19.51	10.26	0.1020	10.02
8EOU27	485	25	1802	0.896	138.4	−0.01	−2.02	2.16	0.0187	2.00

Table 8 BACT flutter test cases

Test case no.	Test	Run	Point no.	M	q, psf	α, deg	Flutter f, Hz	k	Type of flutter
8EFC1	502	25	1438	0.631	158.2	1.64	4.31	0.0574	Classical
8EFC2	502	25	1394	0.747	151.6	1.78	4.14	0.0470	Classical
8EFC3	502	27	1524	0.770	145.2	1.72	4.19	0.0458	Classical
8EFC4	502	26	1469	0.793	146.5	1.81	4.13	0.0439	Classical
8EFC5	502	28	1685	0.801	151.7	2.09	4.17	0.0436	Classical
8EFC6	502	26	1472	0.804	149.9	1.86	4.10	0.0430	Classical
8EFC7	502	26	1477	0.842	161.1	1.83	4.20	0.0420	Classical
8EFC8	502	25	1405	0.859	191.8	1.85	4.10	0.0408	Classical
8EFP1	485	36	2324	0.928	163.7	−0.06	3.37	0.0304	Plunge
8EFP2	485	41	2490	0.935	124.2	−0.06	3.31	0.0299	Plunge
8EFP3	485	33	2240	0.937	133.8	0.03	3.27	0.0294	Plunge
8EFP4	485	41	2488	0.939	124.7	−0.05	3.21	0.0289	Plunge
8EFS1	485	43	2648	0.768	124.2	6.34	4.77	0.0520	Stall
8EFS2	485	42	2571	0.799	126.9	5.43	4.83	0.0506	Stall
8EFS3	485	36	2332	0.799	137.6	5.15	4.74	0.0497	Stall

Table 9 Test cases for forced response with trailing-edge control surface on PAPA, $\delta_{us_0} = \delta_{te_0} = 0$

Test case no.	Test	Run	Point no.	M	q, psf	α, deg	δ_{te}, deg	k	f, Hz
8ERT1	485	38	2377	0.648	112.6	2.02	1.56	0.0445	3.45
8ERT2	485	38	2380	0.649	113.0	2.02	4.08	0.0579	4.50
8ERT3	485	43	2618	0.771	123.6	1.99	1.04	0.0374	3.44
8ERT4	485	43	2619	0.770	123.4	1.98	2.07	0.0467	4.30
8ERT5	485	42	2573	0.796	126.4	4.94	1.05	0.0492	4.69
8ERT6	485	42	2551	0.798	125.0	2.09	2.06	0.0362	3.45
8ERT7	485	42	2553	0.795	124.5	2.09	4.09	0.0456	4.32
8ERT8	485	46	2723	0.875	129.5	2.02	1.04	0.0333	3.44
8ERT9	485	46	2724	0.879	130.5	1.96	4.07	0.0450	4.69

for angles of attack of zero and 4 deg. Note that the transition strip (at 5% chord) has an influence on the first transducer downstream of the strip. The effect varies with angle of attack and other test conditions.

The test cases for static angle of attack, static trailing-edge control surface deflection, and static upper-surface spoiler deflection are presented in Tables 3–5, respectively. An example of an application of BACT data is given in Fig. 1. Static pressures are shown for $\alpha = 4$ deg and $\delta_{te} = -10$ deg at $M = 0.65$ and 0.75 and are compared with linear theory programs.[35,36] Significant transonic effects are shown at the higher Mach number over the forward portion of the chord. One feature of the data set is an irregular pressure distribution at the spoiler hinge line that can be seen in Fig. 1b. This feature is possibly related to the geometric details of the hinge line area or to a small flow through the hinge line.

The test cases for harmonic oscillation of the trailing-edge control surface are given in Table 6 and for upper spoiler oscillations in Table 7. There was no provision for oscillating the main wing and no test cases are included for an open lower surface spoiler. Measured pressure data for test case 8EOT31, a trailing-edge control surface oscillation case, are shown in Fig. 2 for the 0.60-span station. The mean pressure during oscillation is shown in Fig. 2a, and the in-phase and out-of-phase components of pressure as referenced to control position are presented in Figs. 2b and 2c. Large unsteady pressure components are evident both near the hinge line at an x/c of 0.75 and at the shock, which is located near an x/c of 0.30.

The measured flutter points are shown in Fig. 3 in terms of flutter dynamic pressure and flutter frequency vs Mach number and for zero control surface deflections. The classical flutter boundary is shown as a conventional boundary vs Mach number with a minimum near $M = 0.77$ and a subsequent rise. Both the classical flutter boundary and the plunge instability are at small angles of attack,

Table 10 Test cases for forced response with upper surface spoiler on PAPA, $\delta_{te_0} = 0$

Test case no.	Test	Run	Point no.	M	q, psf	α, deg	δ_{us0}, deg	δ_{us}, deg	k	f, Hz
8ERU1	485	39	2434	0.649	116.3	1.89	−10.03	1.00	0.0452	3.50
8ERU2	485	39	2435	0.649	115.7	1.90	−10.02	2.07	0.0582	4.50
8ERU3	485	43	2630	0.768	123.5	1.92	−4.97	2.11	0.0375	3.44
8ERU4	485	43	2631	0.770	124.0	1.93	−4.97	0.99	0.0469	4.32
8ERU5	485	42	2587	0.799	127.7	5.24	−5.09	1.00	0.0504	4.81
8ERU6	485	42	2562	0.795	125.6	2.04	−5.07	2.07	0.0382	3.63
8ERU7	485	42	2563	0.800	126.7	2.02	−5.07	2.05	0.0452	4.32
8ERU8	485	46	2729	0.873	130.2	1.99	−5.07	4.15	0.0332	3.44
8ERU9	485	46	2730	0.874	130.3	2.00	−5.07	4.16	0.0452	4.69

but the stall flutter points are at angles of attack on the order of 5 deg. Thus, α is an independent variable for stall flutter that is not shown in Fig. 3. The stall flutter frequencies are higher than those for classical flutter and are near the pitch frequency (Fig. 3b). However, the frequency of the plunge instability is essentially at the plunge frequency as shown in Fig. 3b. The plunge instability occurs near zero lift, and it was found that opening the upper spoiler a small amount would suppress it. Earlier investigations could go around it by going to a higher angle of attack. Cases for all three types of flutter are selected and are listed in Table 8. The majority of the flutter points are included as test cases, except for nearly coincident points. For the flutter cases, calculations for flutter can be made and compared with measured boundaries. However, the model can be also forced to duplicate the measured combined pitch and plunge motions and the pressures compared directly. Only first harmonics are included in the data set, but time histories have been archived. In addition to the flutter cases, some aeroelastic test cases are included in Tables 9 and 10 for dynamic response measurements of the model on the PAPA mount during forced oscillations of the control surfaces at constant frequency. Again, calculations can be made that include the structural response or that use the measured motion.

Note that all of the tests for BACT were conducted with the heavy gas R-12 as the test medium. The ratio of specific heats γ is calculated to be 1.132–1.135 for the conditions of the test assuming 0.99 for the fraction of heavy gas in the heavy gas–air mixture. A value of 1.132 is suggested for use in computational comparisons. The corresponding value of Prandtl number is calculated to range from 0.77 to 0.78 for the conditions of this test.

Conclusions

Unsteady aerodynamic and aeroelastic computational test cases have been selected from the extensive data set for the BACT model. These test cases are also included in a recent compendium of unsteady aerodynamic test cases. An overview of the test cases that have been selected to illustrate critical trends is given that includes a test case numbering system to facilitate reference to the individual cases in computational efforts. Data sets are selected for trailing-edge control surface oscillations and upper-surface spoiler oscillations for a range of Mach numbers, angle of attack, and static control deflections. Cases are also selected for static angles of attack, static trailing-edge control surface deflections, and static upper-surface spoiler deflections for a range of conditions near those for the oscillation cases. The aeroelastic test cases include classical flutter, stall flutter, and plunging flutter. Dynamic response measurements test cases for oscillations of the controls on the flexible mount are also incorporated.

References

[1]Bennett, R. M., Eckstrom, C. V., Rivera, J. A., Dansberry, B. E., Farmer, M. G., and Durham, M. H., "The Benchmark Aeroelastic Models Program—Description and Highlights of Initial Results," *Transonic Unsteady Aerodynamics and Aeroelasticity*, CP-507, AGARD, 1992; also NASA TM-104180, 1991.

[2]Durham, M. H., Keller, D. F., Bennett, R. M., and Wieseman, C. D., "A Status Report on a Model for Benchmark Active Controls Testing," AIAA Paper 91-1011, April 1991; also NASA TM-107582, 1991.

[3]Rivera, J. A., Jr., Dansberry, B. E., Durham, M. H., Bennett, R. M., and Silva, W. A., "Pressure Measurements on a Rectangular Wing with a NACA 0012 Airfoil During Conventional Flutter," NASA TM-104211, July 1992.

[4]Rivera, J. A., Dansberry, B. E., Bennett, R. M., Durham, M. H., and Silva, W. A., "NACA 0012 Benchmark Model Experimental Flutter Results with Unsteady Pressure Distributions," AIAA Paper 92-2396, April 1992; also NASA TM-107581, March 1992.

[5]Rivera, J. A., Dansberry, B. E., Farmer, M. G., Eckstrom, C. V., Seidel, D. A., and Bennett, R. M., "Experimental Flutter Boundaries with Unsteady Pressure Distributions for the NACA 0012 Benchmark Model," AIAA 91-1010, 1991; also NASA TM-104072, 1991.

[6]Perry, B., III, Cole, S. R., and Miller, G. D., "Summary of an Active Flexible Wing Program," *Journal of Aircraft*, Vol. 32, No. 1, 1995, pp. 10–15.

[7]Sandford, M. C., Abel, I., and Gray, D. L., "Development and Demonstration of a Flutter-Suppression System Using Active Controls," NASA TR-R-450, 1974.

[8]Scott, R. C., Hoadley, S. T., Wieseman, C. D., and Durham, M. H., "Benchmark Active Controls Technology Model Aerodynamic Data," AIAA Paper 97-0829, Jan. 1997; also *Journal of Guidance, Control, and Dynamics*, Vol. 23, No. 5, 2000, pp. 914–921.

[9]"Compendium of Unsteady Aerodynamic Measurements," AGARD Rept. 702, Aug. 1982.

[10]"Compendium of Unsteady Aerodynamic Measurements, Addendum No. 1," AGARD Rept. 702, May 1985.

[11]Ruiz-Calavera, L. P. (ed.), "Verification and Validation Data for Computational Unsteady Aerodynamics Codes," Research and Technology Organization TR-26, 2000.

[12]Bartels, R. E., and Schuster, D. M., "Comparison of Two Navier–Stokes Aeroelastic Methods Using BACT Benchmark Experimental Data," *Journal of Guidance, Control, and Dynamics* (to be published).

[13]Bartels, R. E., and Schuster, D. M., "A Comparison of Two Navier–Stokes Aeroelastic Methods Using BACT Benchmark Experimental Data," AIAA Paper 99-3157, June 1999.

[14]Schuster, D. M., Beran, P. S., and Huttsell, L. J., "Application of the ENS3DAE/Navier–Stokes Aeroelastic Method," *Numerical Unsteady Aerodynamics and Aeroelastic Simulation*, Paper 3 in Rept. 822, AGARD, March 1998.

[15]Roughen, K. M., Baker, M. L., and Fogarty, T., "CFD and Doublet-Lattice Calculation of Unsteady Control Surface Aerodynamics and Correlation with Wind-Tunnel Test," AAIA Paper 99-1469, Jan. 1999.

[16]Waszak, M. R., "Modeling the Benchmark Active Control Technology Wind-Tunnel Model for Active Control Design Applications," NASA TP-1998-206270, June 1998.

[17]Waszak, M. R., "Modeling the Benchmark Active Controls Technology Wind-Tunnel Model for Application to Flutter Suppression," AIAA 96-3437, July 1996.

[18]Waszak, M. R., and Fung, J., "Parameter Identification and Analysis of Actuators for the BACT Wind-Tunnel Model," AIAA Paper 96-3362, July 1996.

[19]Lichtenwalner, P., Little, G., and Scott, R., "Adaptive Neural Control of Aeroelastic Response," Society of Photo-Optical Instrumentation Engineers, Paper 2717–12, Feb. 1996.

[20]Lichtenwalner, P., Little, G., Pado, L., and Scott, R., "Adaptive Neural Control for Active Flutter Suppression," *Proceedings of the ASME Fluids Engineering Div. FED*, Vol. 242, 1996.

[21]D'Cruz, J., "A Determination of the External Forces Required to Move the Benchmark Active Controls Testing Model in Pure Plunge and Pure Pitch," NASA TM-107743, July 1993.

[22]"The Langley Transonic Dynamics Tunnel," Aeroelasticity Branch, NASA Langley Research Center, LWP-799, Hampton, VA, Sept. 1969.

[23]Cole, S. R., and Rivera, J. A., Jr., "The New Heavy Gas Testing Capability in the NASA Langley Transonic Dynamics Tunnel," Royal Aeronautical Society, Paper 4, April 1997.

[24]Corliss, J. M., and Cole, S. R., "Heavy Gas Conversion of the NASA Langley Transonic Dynamics Tunnel," AIAA Paper 98-2710, June 1998.

[25]Cole, P. H., "Wind Tunnel Real-Time Data Acquisition System," NASA TM-80081, 1979.

[26]Bryant, C., and Hoadley, S. T., "Open Architecture Dynamic Data System at Langley's Transonic Dynamics Tunnel," AAIA Paper 98-0343, Jan. 1998.

[27]Wieseman, C. D., and Hoadley, S. T., "Versatile Software Package for Near Real-Time Analysis of Experimental Data," AIAA Paper 98-2722, June 1999.

[28]Dougherty, N. S., Jr., "Influence of Wind Tunnel Noise on the Location of Boundary-Layer Transition on a Slender Cone at Mach Numbers from 0.2 to 5.5. Volume I.—Experimental Methods and Summary of Results. Volume II.—Tabulated and Plotted Data," Arnold Engineering Development Center AEDC-TR-78-44, March 1980.

[29]Dougherty, N. S., Jr., and Fisher, D. F., "Boundary-Layer Transition on a 10-Deg Cone, Wind Tunnel/Flight Correlation," AIAA Paper 80-0154, Jan. 1980.

[30]Sleeper, R. K., Keller, D. F., Perry, B., III, and Sandford, M. C., "Characteristics of Vertical and Lateral Tunnel Turbulence Measured in Air in the Langley Transonic Dynamics Tunnel," NASA TM-107734, March 1993.

[31]Schuster, D. M., "Aerodynamic Measurements on a Large Splitter Plate for the NASA Langley Transonic Dynamics Tunnel" (submitted for publication).

[32]Farmer, M. G., "A Two-Degree-of-Freedom Flutter Mount System with Low Damping for Testing Rigid Wings at Different Angles of Attack," NASA TM-83302, 1982.

[33]Farmer, M. G., "Mount System for Testing Flutter," U.S Patent 4,475,385, 9 Oct. 1984.

[34]Dansberry, B. E., Durham, M. H., Bennett, R. M., Turnock, D. L., Silva, W. A., and Rivera, J. A., Jr., "Physical Properties of the Benchmark Models Program Supercritical Wing," NASA TM-4457, Sept. 1993.

[35]Rowe, W. S., Redman, M. C., Ehlers, F. E., and Sebastian, J. D., "Prediction of Unsteady Aerodynamic Loadings Caused by Leading Edge and Trailing Edge Control Surface Motions in Subsonic Compressible Flow—Analysis and Results," NASA CR-2543, May 1975.

[36]Giesing, J. P., Kalman, T. P., and Rodden, W. P., "Subsonic Unsteady Aerodynamics for General Configurations, Part I—Vol. I—Direct Application of the Nonplanar Doublet Lattice Method," Air Force Flight Dynamics Lab., AFFDL-TR-71-5, Wright-Patterson AFB, OH, Nov. 1971.